$E2$ Interference Effects in the $^{12}C(\alpha, \gamma_0)^{16}O$ Reaction

D. B. Sayre,[*,†] C. R. Brune,[‡] D. E. Carter, D. K. Jacobs, T. N. Massey, and J. E. O'Donnell
Ohio University, Athens, Ohio 45701, USA
(Received 4 May 2012; published 3 October 2012)

The $E1$-$E2$ interference sign between the $E_{\text{c.m.}} = 2.68 - \text{MeV}$ $E2$ resonance and an underlying $E1$ strength has been measured for the first time. An $E1$-$E2$ asymmetry parameter of $a = 0.07 \pm 0.05$ was extracted from the thick-target γ-ray yields of the narrow resonance at angles of 45° and 135°. The positive sign of a corresponded to constructive interference at forward angles and, further, allowed the interference between the resonance and an $E2$ background to be identified as constructive below the resonance energy. The $E2$-$E2$ interference was then used to evaluate the global S_{E2} data within the vicinity of the resonance $2.5 \leq E_{\text{c.m.}} \leq 3.0$ MeV. An analysis of the global S_{E2} data that agreed with the interference scenario has determined the $E2$-$E2$ interference scheme of the 4.34-MeV resonance and background, resulting in a value of $S_{E2}(300) = 62^{+9}_{-6}$ keV b.

DOI: 10.1103/PhysRevLett.109.142501 PACS numbers: 26.20.−f, 25.55.−e, 23.20.En, 29.85.−c

The helium-burning stage of red giant stars is dominated by the triple-α-particle process($3\alpha \rightarrow {}^{12}C$) and the $^{12}C(\alpha, \gamma)^{16}O$ reaction, making a precise understanding of both reactions essential for modeling the evolution of stars from this stage and beyond [1,2]. Despite four decades of experimental investigations, the uncertainty associated with the $^{12}C(\alpha, \gamma)^{16}O$ reaction continues to be an obstacle. An uncertainty of $\leq 10\%$ in the astrophysical $^{12}C(\alpha, \gamma)^{16}O$ cross section is needed to advance the modeling [3], yet even the smallest error bars reported thus far greatly exceed that value [4].

At helium-burning energies of $E = 300$ keV (throughout this Letter we refer to center-of-mass energies in the $^{12}C + \alpha$ channel), the reaction is governed by ground-state $E1$ and $E2$ captures through $J^\pi = 1^-$ and 2^+ resonances, with cascades being about an order of magnitude smaller. Presently, the cross section [or S factor at 300 keV, $S(300)$] can only be determined through a combination of experimental data and theoretical extrapolation; direct measurements have been limited to energies $\gtrsim 1$ MeV for technological reasons. Indirect approaches have been investigated to constrain the low-energy extrapolation, such as $^{12}C + \alpha$ elastic scattering [4–6], the ^{16}N β-delayed α-decay spectrum [7–10], α-transfer on ^{12}C with beams of Li isotopes [11,12], and cascade transitions through the 6.92-MeV state of ^{16}O [13,14]. However, recent ground-state $S_{E2}(300)$ values have ranged from 30–60% of $S(300)$ [4,11,14,15], having an unsatisfactory dependence on experimental data sets and assumptions made in the analysis.

A notable contributor to the large variation in $S_{E2}(300)$ values is the systematic errors in the global data. Roughly a third of the S_{E2} data are located in the vicinity of the narrow 2.68-MeV (2^+) resonance $2.5 \leq E \leq 3.0$ MeV. Here, the $E2$ cross section is a coherent sum of amplitudes from the 2.68-MeV resonance and an underlying component resulting from other 2^+ resonances and external capture. Measurements of the cross section around the resonance become acutely sensitive to the beam energy distribution within the target. Another complication is that the target thickness can change during the measurements. As a consequence, many of the data have unreported systematic errors and this poses a serious challenge for any reliable analysis. It has been pointed out [16] that most of the existing S_{E2} datasets result in conflicting interference scenarios between the resonance and underlying $E2$ component. This unphysical result is also found in a more recent data set from a group that has reported making the target corrections [17].

Some groups [18,19] have simply chosen not to fit the global S_{E2} data within the vicinity of the 2.68-MeV resonance. Although this approach avoids the mentioned systematic errors, it limits the constraints that can be placed on the fit. For example, data around the 2.68-MeV resonance are key to identifying the $E2$-$E2$ interference scheme between the 4.34-MeV (2^+) resonance and background component. This is important because the interferences of resonances, like their decay proprieties, need to be specified for the extrapolation. A significant uncertainty in previous $S_{E2}(300)$ analyses [4,11] arose from the inability to resolve how the 4.34-MeV resonance interfered with the background. In accounting for this ambiguity, Ref. [4] averaged the values, $S_{E2}(300) = 49^{+7}_{-9}$ and 58^{+8}_{-11} keV b, from the different interference scenarios to obtain $S_{E2}(300) = 53^{+13}_{-18}$ keV b. We address this uncertainty by measuring a new observable that independently determines the interference scenario between the 2.68-MeV resonance and the underlying $E2$ amplitude. Having established the energy dependence of the $E2$ cross section in the vicinity of the resonance, we then evaluate the global S_{E2} data and eliminate those with systematic discrepancies.

It has been shown [16] that the angular distribution of the integrated γ-ray yield from the 2.68-MeV resonance can be used to determine its $E2$-$E2$ interference scheme. Along with the energy-dependent $E2$-$E2$ interference in

the angle-integrated cross section, there is an angle-dependent interference between an $E1$ background and the $E2$ resonance. The relative phase of the $E1$ and $E2$ background amplitudes is well known from angular distribution measurements below the resonance [15,20,21]. Based on this information, a determination of the $E1$-$E2$ relative phase using the integrated yield of the resonance also determines the relative phase of the $E2$-$E2$ interference. Ref. [16] has derived an expression for the angular distribution of the integrated yield

$$W(\theta) = 1 + \frac{5}{7}P_2 - \frac{12}{7}P_4 + a(P_1 - P_3), \qquad (1)$$

which consists of Legendre polynomials $P_\ell = P_\ell(\cos\theta)$ and a parameter a that leads to an asymmetry about 90°. The magnitude of a can be calculated from existing data, $|a| = 0.08 \pm 0.01$ [16], but the sign of a can not. Depending on whether a is positive or negative, the $E2$-$E2$ interference will be constructive or destructive below the resonance energy. We report in this Letter the first measurement of the asymmetry parameter, and find its sign to be positive.

Measurements of the $^{12}C(\alpha, \gamma)^{16}O$ reaction were performed with the 4.5-MV tandem Van de Graaff accelerator at Ohio University, where 200-pnA beams of α particles bombarded a $30 - \mu g/cm^2$ carbon foil composed of >99.9% ^{12}C. The target was sufficiently thick to integrate the 2.68-MeV resonance ($\Gamma = 0.6 \pm 0.1$ keV [22]) while restricting both nonresonant and background reactions. To help preserve the target properties during the experiment, a liquid-nitrogen cold trap was installed around the target for suppressing the buildup of carbon (with natural isotopic composition) on its surface.

Throughout the experiment the elastic scattering spectrum from the target was monitored with a silicon surface-barrier detector fixed at 144°. The 2.68-MeV resonance appeared in the spectrum, and this was utilized to tune the beam energy until it was centered within the target. Also, a $1 - \mu g/cm^2$ layer of gold was deposited over the target. Detection of elastically scattered α particles from gold provided a measure of the number incident to the target, which supplemented the information obtained with a Faraday cup.

The $\approx$10 MeV γ rays from the ground-state decay of the 2.68-MeV resonance were measured with a $10 - \text{cm} \times 10 - \text{cm}$ cylindrical bismuth germanate (BGO) detector, which was both actively and passively shielded from the ambient room background. In a compromise between detection efficiency and the importance of finite size and misalignment corrections, the front face of the BGO detector was placed 20 cm away from the target. The detector was placed between several guide rails atop a rotatable platform, so that its position could be reproduced for measurements at different angles. The rotation axis of this platform was aligned with the beam-target intersection to submillimeter precision using an *in situ* γ-ray source, created by activating a sodium-tungstate target through the $^{23}Na(d, p)^{24}Na$ reaction [23]. Additionally, measurements of the $^{12}C(\alpha, \gamma)^{16}O$ reaction were performed on both sides of the beamline to mitigate the effects from beam wander on the target.

Extraction of the γ-ray yields involved fitting the $^{12}C(\alpha, \gamma)^{16}O$ spectra with the combination of a Monte Carlo signal and several measured backgrounds (see Fig. 1). The simulated $^{12}C(\alpha, \gamma)^{16}O$ signal was produced with the Geant4 [24] toolkit and considered the reaction kinematics, γ-ray angular distribution, attenuation of the target chamber and cold trap, and detector efficiency. Together with the ambient background there was a beam-induced contribution from the $^{13}C(\alpha, n)^{16}O$ reaction. Its spectra were acquired in a separate experiment that replicated the beam energy, target thickness, and detector positions of the $^{12}C(\alpha, \gamma)^{16}O$ measurements, except with a 99% ^{13}C target. The scaled backgrounds were subtracted from the $^{12}C(\alpha, \gamma)^{16}O$ spectra, and the remaining counts within a 9-to-10 MeV region of interest were integrated. In addition to the statistics from the extracted yields, systematic errors were considered for the energy miscalibration, detector misalignment, fit region, beam energy shifts, and region of interest. The ratio of the 45° to 135° yields, each normalized by the number of incident particles, was related to the $E1$-$E2$ asymmetry parameter through the simulations. Two separate measurements of the ratio gave values of $a = 0.09 \pm 0.07$ and 0.05 ± 0.07, resulting in a weighted average of $a = 0.07 \pm 0.05$ (a systematic error of 0.02 was common to both measurements and has been added in quadrature to the combined statistical error). The

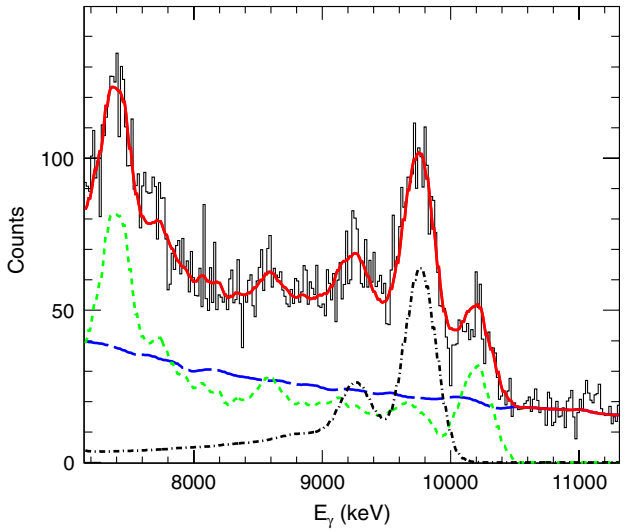

FIG. 1 (color online). A fit to the 135° γ-ray yield from the first $^{12}C(\alpha, \gamma)^{16}O$ experiment. The solid (red) curve was the sum of three contributions: an ambient room background shown as a long dashed (blue) curve, a beam-induced background given by the short dashed (green) curve, and a Monte Carlo signal that corresponds to the dash-dot (black) curve.

positive value of a corresponded to constructive $E2$-$E2$ interference below the 2.68-MeV resonance.

Our experimental result was then used to constrain an R-matrix [19,25] fit with the global S_{E2} data and the d-wave elastic-scattering phase shifts of Ref. [6]. This analysis utilized the alternative parametrization of the R-matrix [26] so that experimental quantities could be directly included in the analysis. R-matrix parameters were determined from the minimization of

$$\chi^2 = \sum_{i=1}^{N_e}\left[\sum_{j=1}^{N_i}\left(\frac{\mathcal{N}_i y_j - t_j}{\mathcal{N}_i \sigma_j}\right)^2 + \left(\frac{\mathcal{N}_i - 1}{s_i}\right)^2\right], \quad (2)$$

with Minuit [27]. Eq. (2) is summed over all experiments N_e, each having a number N_i of data points. Here, y_j and t_j are the experimental and theoretical values at data point j, and σ_j is the statistical uncertainty associated with y_j. An adjustable normalization $\mathcal{N}_i$ is determined for each S_{E2} data set (the phase shifts are not rescaled) by minimizing the second term $\chi^2_{\mathcal{N}}$. Normalization uncertainties s_i are taken as $s_i \to \infty$ for experiments that have normalized their data to other measurements, allowing their $\mathcal{N}_i$ to float freely. Otherwise, s_i is taken to be its reported value (see Table II). The only exception being the 6% normalization uncertainty of Ref. [20], which was determined in part by using a derived quantity from another analysis. Instead, the 13% value determined independently by that experiment, from a measurement of the cross section around the 2.42-MeV resonance, was used. Following Refs. [4,8–11,14], the acceptable $S_{E2}(300)$ range from the fit was determined by $\chi^2 \leq \chi^2_{\min}(1 + 9/\nu)$, with ν being the number of degrees of freedom in the fit.

Five 2^+ levels were considered in the R-matrix: a background pole and physical resonances at -0.245, 2.68, 4.34, and 5.86 MeV. Of these levels there were 7 adjustable parameters: the energy and widths of the background pole, the energy and α-particle width of the 4.34-MeV resonance, and the asymptotic normalization coefficients (ANC) of the subthreshold resonance and final state (-7.162 MeV). All other decay properties were fixed with experimental values. Resonance energies and α-particle widths were taken from Refs. [4,6], except for the α-particle width of 2.68-MeV resonance [22]. Radiative widths for the -0.245, 2.68, 4.34, and 5.86 MeV resonances were obtained from Refs. [32–35], respectively. The interference signs of the 2.68-MeV and subthreshold resonances were fixed in every fit; signs for other radiative width parameters were investigated individually.

Fits of two types were considered to the global S_{E2} data: (a) only the S_{E2} data ≤ 2.5 MeV and (b) all data that followed the determined 2.68-MeV interference scenario (in addition to the data ≤ 2.5 MeV). Eleven data points [36] within the $2.5 \leq E \leq 3.0$ MeV region that did not follow the interference scenario were eliminated according to Chauvanet's criterion [37].

The fits outlined above represent two approaches to deal with the systematic errors around the 2.68-MeV resonance, with the second signifying a new way to include the data around the 2.68-MeV resonance. For reference, both fits are shown in Fig. 2. Note: The only difference between the fits of (a) and (b) was that 15 additional S_{E2} data points were included in the latter.

The best fit of type (a), which gave a $\chi^2_{\min} = 202$ for 381 data points, occurred when the 4.34-MeV and subthreshold resonances had opposite interference signs. Although the case having identical signs only raised the total χ^2 by 2, and also fell within the acceptable range from the $\chi^2_{\min}$, $\Delta\chi^2 = 5$. The best fit of type (b) resulted in a $\chi^2_{\min}$ of 218 for 396 data points. Again, the best fit occurred when 4.34-MeV and subthreshold resonances had opposite signs. In Fit (b), however, the other interference scenario could be excluded since it increased the total χ^2 by 10. Fit (a) in Fig. 2 illustrates that the destructive scenario below the 4.34-MeV resonance (identical signs) favors smaller values of S_{E2} above the 2.68-MeV resonance than the constructive one. The additional data of Fit (b) require larger S_{E2} values above the 2.68-MeV resonance, and this leads to an increased background strength for the destructive interference fit. A poorer quality fit to the data below the resonance results from the larger background pole.

We also find the 4.34-MeV interference scenario from our analysis confirmed in recently reported S_{E2} measurements [31]. To further constrain our final analysis, we have included this new data set. Table I lists R-matrix parameters from the best fit, which gave a $\chi^2_{\min} = 226$ for 399 data points and resulted in a value of $S_{E2}(300) = 62^{+9}_{-6}$ keV b. A channel radius of 5.5 fm was used in all fits [4] because larger channel radii were found to require additional background levels. In the Table, radiative widths for the ground-state transition $\Gamma_{\gamma 0}$ are accompanied by their interference

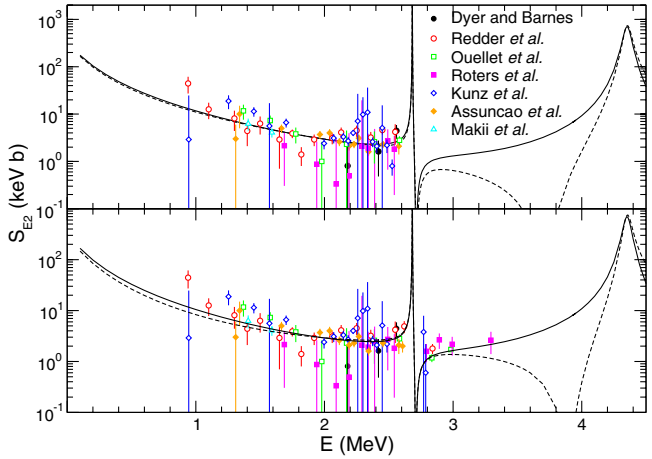

FIG. 2 (color online). Fits (a) (top panel) and (b) (bottom panel) to the global S_{E2} data. The solid (dashed) line represents the fit assuming the opposite (same) interference signs for the 4.34-MeV and subthreshold resonances.

TABLE I. The R-matrix parameters from the best fit. Fixed parameters are shown in parentheses, and the signs are discussed in the text. The ANC is reported instead of an α-particle width for levels below the $\alpha + {}^{12}$C threshold.

$\lambda\ell$	E_λ (MeV)	ANC (fm $-$ 1/2)	Γ_α (keV)	$\Gamma_{\gamma 0}$ (meV)
10	($-$ 7.162)	7.09×10^2		
12	($-$ 0.245)	1.59×10^5		(97)
22	(2.683)		(0.6)	($-$ 5.9)
32	4.340		82.9	($-$ 610)
42	(5.857)		(350)	(700)
52	21.59		129	1.31×10^5

signs. A sign is also considered for the ANC of the final state. It should be mentioned that the interference scheme of the 5.86-MeV resonance could not be determined here, as a fit with the negative sign only increased χ^2 by 3. The asymmetric error in our result comes from the fit with the negative interference sign. An uncertainty of 3 keV b from the fixed parameters, which was determined by performing separate fits for each parameter at its 1σ deviation, has also been considered.

Table II provides fit details, such as the normalizations $\mathcal{N}_i$ and χ^2 per data set χ^2_i. The individual data sets appear to be well described by the global fit, with the possible exception of Ref. [20] which gives a rather large χ^2_i/N_i value. It should also be noted that the χ^2_i/N_i value of Ref. [6] is unrealistically small.

Our result of $S_{E2}(300) = 62^{+9}_{-6}$ keV b, is heavily dependent upon the elastic scattering data of Refs. [4,6]. However, we have repeated the analysis with an alternative set of phase shift data [5] and found consistent results, $S_{E2}(300) = 38^{+34}_{-25}$ keV b, albeit with much greater uncertainty. In comparison to the $S_{E2}(300) = 53^{+13}_{-18}$ keV b value reported by Ref. [4], the present result is both larger and with significantly smaller uncertainty. The main distinction between results comes from our ability to exclude the destructive interference scenario for the 4.34-MeV resonance; if the destructive interference scenario for the 4.34-MeV resonance is eliminated from the analysis of Ref. [4], a comparable result is obtained. Smaller changes arise from the adjustable data set normalizations in our analysis and the inclusion of newer S_{E2} data [15,17,30,31]. Other analyses that did not make use of the high-precision phase shifts, but instead relied on the either the α-transfer or the 6.92-MeV cascade data to determine the ANC of the -0.245 $-$ MeV resonance, determined $S_{E2}(300)$ values of 44^{+16}_{-23} keV b [11] and 95 ± 24 keV b [14], respectively. Future investigations should be considered to understand the source of the discrepancy in ANC values.

TABLE II. Details of the fit to each data set. The data type has been indicated as either d-wave phase shift δ_2 or ground-state $E2$ S-factor S_{E2}; other columns of the Table were discussed in the text.

Ref.	Type	N_i	s_i	$\mathcal{N}_i$	$\chi^2_{\mathcal{N}}$	χ^2_i
[6]	δ_2	321				131.9
[15]	S_{E2}	19	0.11	0.90	0.9	22.8
[17]	S_{E2}	12	0.09	1.07	0.6	16.9
[20]	S_{E2}	17	0.13	0.96	1.2×10^{-2}	30.2
[28]	S_{E2}	13	∞	1.04		7.3
[29]	S_{E2}	3	0.10	1.01	1.0×10^{-2}	3.1
[21]	S_{E2}	9	∞	0.95		6.8
[30]	S_{E2}	2	0.05	1.00	7.0×10^{-6}	0.3
[31]	S_{E2}	3	0.05	1.00	4.0×10^{-5}	6.8

We have experimentally determined the $E2$-$E2$ interference scheme of the 2.68-MeV resonance and presented a way to include data within $2.5 \leq E \leq 3.0$ MeV region based upon that determination. The S_{E2} data within this region were found to resolve the $E2$-$E2$ interference scheme of the 4.34-MeV resonance – a significant uncertainty in previous analyses [4,11] of the ground-state S_{E2} factor. Combining our $S_{E2}(300)$ value with an average of Refs. [8,10], $S_{E1}(300) = 83 \pm 22$ keV b, and an estimate of the cascades, 16 ± 16 keV b [38], gives a total of $S(300) = 161 \pm 28$ keV b. This result is consistent with the 170 ± 20 keV b [3] value obtained by matching supernova nucleosynthesis calculations with the solar-system abundances.

We acknowledge the work of D. Shafer and C. Dodson in the design and fabrication of equipment, thank D. C. Ingram for assistance with the experimental setup, and appreciate the help with accelerator operations from S. Ahktar, Y. Byun, S. Dhakal, C. Parker, A. Ramirez, and A. Voinov. This work was supported in part by the U. S. Department of Energy under grant numbers DE-FG02-88ER40387 and DE-FG52-09NA29455.

*Present address: Lawrence Livermore National Laboratory, Livermore, California 94550, USA.
†sayre4@llnl.gov
‡brune@ohio.edu

[1] T. A. Weaver and S. E. Woosley, Phys. Rep. **227**, 65 (1993).
[2] C. Tur, A. Heger, and S. M. Austin, Astrophys. J. **671**, 821 (2007).
[3] S. E. Woosley, A. Heger, and T. A. Weaver, Rev. Mod. Phys. **74**, 1015 (2002).
[4] P. Tischhauser *et al.*, Phys. Rev. Lett. **88**, 072501 (2002).
[5] R. Plaga, H. W. Becker, A. Redder, C. Rolfs, H. P. Trautvetter, and K. Langanke, Nucl. Phys. **A465**, 291 (1987).
[6] P. A. Tischhauser *et al.*, Phys. Rev. C **79**, 055803 (2009), we fit all phase shifts except those within the 2.6–2.8 MeV region.
[7] L. Buchmann *et al.*, Phys. Rev. Lett. **70**, 726 (1993).
[8] R. E. Azuma *et al.*, Phys. Rev. C **50**, 1194 (1994).
[9] X. D. Tang *et al.*, Phys. Rev. Lett. **99**, 052502 (2007).
[10] X. D. Tang *et al.*, Phys. Rev. C **81**, 045809 (2010).

[11] C. R. Brune, W. H. Geist, R. W. Kavanagh, and K. D. Veal, Phys. Rev. Lett. **83**, 4025 (1999).
[12] A. Belhout *et al.*, Nucl. Phys. **A793**, 178 (2007).
[13] L. Buchmann, Phys. Rev. C **64**, 022801(R) (2001).
[14] C. Matei, C. R. Brune, and T. N. Massey, Phys. Rev. C **78**, 065801 (2008).
[15] R. Kunz, M. Jaeger, A. Mayer, J. W. Hammer, G. Staudt, S. Harissopulos, and T. Paradellis, Phys. Rev. Lett. **86**, 3244 (2001).
[16] C. R. Brune, Phys. Rev. C **64**, 055803 (2001).
[17] M. Assunção *et al.*, Phys. Rev. C **73**, 055801 (2006).
[18] B. W. Filippone, J. Humblet, and K. Langanke, Phys. Rev. C **40**, 515 (1989).
[19] F. C. Barker and T. Kajino, Aust. J. Phys. **44**, 369 (1991).
[20] A. Redder, H. W. Becker, C. Rolfs, H. P. Trautvetter, T. R. Donoghue, T. C. Rinckel, J. W. Hammer, and K. Langanke, Nucl. Phys. **A462**, 385 (1987).
[21] J. M. Ouellet *et al.*, Phys. Rev. C **54**, 1982 (1996).
[22] A. McDonald, T. K. Alexander, J. R. Beene, J. C. Hardy, K. P. Jackson, and H. B. Mak, Nucl. Phys. **A287**, 189 (1977).
[23] D. B. Sayre, Ph.D. thesis, Ohio University 2011, http://etd.ohiolink.edu.
[24] S. Agostinelli *et al.*, Nucl. Instrum. Methods Phys. Res., Sect. A **506**, 250 (2003).
[25] A. Lane and R. Thomas, Rev. Mod. Phys. **30**, 257 (1958).
[26] C. R. Brune, Phys. Rev. C **66**, 044611 (2002).
[27] F. James, *Minuit: Function Minimization and Error Analysis* (CERN, Geneva, 1994).
[28] G. Roters, C. Rolfs, F. Strieder, and H. P. Trautvetter, Eur. Phys. J. A **6**, 451 (1999).
[29] P. Dyer and C. A. Barnes, Nucl. Phys. **A223**, 495 (1974).
[30] H. Makii, Y. Nagai, T. Shima, M. Segawa, K. Mishima, H. Ueda, M. Igashira, and T. Ohsaki, Phys. Rev. C **80**, 065802 (2009).
[31] D. Schürmann *et al.*, Phys. Lett. B **703**, 557 (2011), we do not fit the four data points over the 4.34-MeV resonance.
[32] R. Moreh, W. C. Sellyey, D. Sutton, and R. Vodhanel, Phys. Rev. C **31**, 2314 (1985).
[33] J. D. Larson and R. H. Spear, Nucl. Phys. **56**, 497 (1964).
[34] F. Brochard, P. Chevallier, D. Disdier, V. Rauch, and F. Scheibling, J. Phys. (Paris) **36**, 113 (1975).
[35] W. M. G. Kernel and U. von Wimmersperg, Nucl. Phys. **A167**, 352 (1971).
[36] We exclude all data above 2.6 MeV from Ref. [17]; the 2.526-MeV data point from Ref. [15]; the 2.83-MeV data point of Ref. [29]; and the 2.78-MeV point of Ref. [20].
[37] P. R. Bevington, *Data Reduction and Error Analysis for the Physical Sciences* (McGraw-Hill, New York 1969).
[38] L. Buchmann, R. E. Azuma, C. A. Barnes, J. Humblet, and K. Langanke, Phys. Rev. C **54**, 393 (1996).